Effect of Finite Plate Length on Supersonic Turbulent Boundary Layer with Large Distributed Surface Injection

FERNANDO L. FERNANDEZ* AND LESTER LEES†
California Institute of Technology, Pasadena, Calif.

The two-dimensional, supersonic, turbulent boundary layer on a finite length flat plate with large injection is analyzed using integral moment methods which include the interaction between the viscous and inviscid flows. Data obtained at $M_\infty = 2.6$ are presented and show agreement with the analysis. As injection is increased, the velocity profiles become inflected, the sonic line moves away from the wall and the flow becomes "subcritical." Under this condition, the effect of termination of injection can be felt upstream of the end of injection. In particular, as injection rates approaching the maximum value which can be entrained by a constant pressure mixing layer are approached, the analysis predicts that virtually the entire blowing region experiences a falling pressure due to the effect of finite length. It is postulated that this effect provides for a smooth transition from a boundary-layer flow to one where mixing is negligible, except in a thin layer near the streamline which divides the injected and freestream gas.

Nomenclature‡

a = speed of sound
B = function defined in Eq. (12)
C_f = skin-friction coefficient $= 2\tau_w/\rho_e u_e^2$
C_p = specific heat at constant pressure
D = function defined in Eq. (28)
f = function defined in Eq. (12)
$\mathfrak{H}$ = $\theta_i/\delta_i{}^*$, form factor
J = integral function $= \dfrac{1}{\delta_i{}^*}\displaystyle\int_0^{\delta_i} \frac{u}{u_e}\left[1-\left(\frac{u}{u_e}\right)^2\right] dY$
K_θ = eddy viscosity coefficient ($\rho^2\epsilon = K_\theta \rho_R{}^2 u_e \theta$)
K = perturbation parameter in Eq. (32)
L = length of porous plate
M = Mach number
m = $[(\gamma-1)/2]M^2$
$N_{1,2,3}$ = functions defined in Eqs. (25–27)
P = static pressure
R = integral function $= \dfrac{2}{\lambda_e}\displaystyle\int_0^{\delta_i} \frac{\tau}{\rho_e u_e{}^2}\frac{\partial(u/u_e)}{\partial Y} dY$
T = static temperature
u = velocity component in x direction
v = velocity component in y direction
x = distance along plate measured from start of porous region
y = distance normal to plate
Y = transformed distance normal to wall, $dY = (a_e\rho/a_2\rho_2)dy$
Z = integral function $= \dfrac{1}{\delta_i{}^*}\displaystyle\int_0^{\delta_i} \frac{u}{u_e} dY$
δ^* = displacement thickness $= \displaystyle\int_0^{\delta}\left(1-\frac{\rho u}{\rho_e u_e}\right) dy$
δ = edge of layer
θ = momentum thickness, $\displaystyle\int_0^{\delta}\frac{\rho u}{\rho_e u_e}\left(1-\frac{u}{u_e}\right) dy$
$\delta_i{}^*$ = transformed displacement thickness, $\displaystyle\int_0^{\delta_i}\left(1-\frac{u}{u_e}\right) dY$
θ^{**} = integral function, $\displaystyle\int_0^{\delta}\frac{\rho u}{\rho_e u_e}\left[1-\left(\frac{u}{u_e}\right)^2\right] dy$
δ_u = integral function, $\displaystyle\int_0^{\delta}\left(1-\frac{u}{u_e}\right) dy$
Θ = induced flow angle at edge, $\tan\Theta = v_e/u_e$
λ_e = $\rho_w v_w/\rho_e u_e$
λ_∞ = $\rho_w v_w/\rho_\infty u_\infty$
η,ξ,σ = transformation functions
μ = viscosity
ψ = stream function, $\partial\psi/\partial y = \rho u$, $\partial\psi/\partial x = -\rho v$
τ = shear stress
ρ = density

Subscripts

w = wall value
e = value at edge of layer
∞ = freestream value
i = transformed quantities
2 = value at reference station (similar region)

1. Introduction

ANALYSES of both laminar and turbulent boundary layers with uniform, distributed surface injection have indicated that if an a priori condition of constant pressure is imposed on a flat surface, a particular value of uniform injection rate exists beyond which no solutions can be obtained.[1,2] These analyses have also shown that the value of injection at which this singularity occurs corresponds very closely to the entrainment rate on the low-speed side of a constant pressure mixing layer. It has been argued that boundary-layer theory is invalid beyond this point and inviscid flow models have been employed to give a description of the flow.[3] These two-dimensional, inviscid solutions can be obtained only for flows with a negative pressure gradient. Furthermore, for subsonic injection these inviscid solutions scale directly with the plate length (i.e., exist only for a finite length porous region) and are uniquely determined by a saddle point singularity which exists at the end of the injection region.

However, for laminar boundary-layer flow, analyses are also available which indicate that for any small, but negative

Presented at the AIAA 7th Aerospace Sciences Meeting, New York, January 20–22, 1969; submitted February 2, 1969; revision received November 25, 1969. Work supported by ARO and ARPA under Contract DA-31-124-ARO(D)-33. The authors would like to acknowledge the help given by G. Emanuel in preparing this manuscript. His probing comments have been very useful.

* Presently Head, Fluid Mechanics Department, The Aerospace Corporation, San Bernardino, Calif. Associate AIAA.
† Professor of Aeronautics. Fellow AIAA.

‡ Bars above quantities denote values for an incompressible flow, $\bar{\rho}$ = constant.

pressure gradient, the boundary-layer equations possess no "blow-off" singularity.[4] For turbulent flow, one expects the same result to hold. The analysis which is required, then, is one which describes the manner in which a boundary layer initially at constant pressure adjusts as injection is increased up to and beyond the constant pressure "blow-off" values. Furthermore, for turbulent flow, quantitative bounds are needed to establish the ranges of injection rate where mixing alone, both pressure gradient and mixing, and only pressure gradient influence the solution (the inviscid limit).

Hence, the question becomes one of determining what mechanism will generate the pressure gradient. A plausible mechanism involves the effect of termination of injection on the flow as a means of inducing a favorable pressure gradient. This effect should be similar to that experienced by a flow approaching a rapid expansion corner. This explanation seems physically appealing since the thickness of the layer itself near the end of injection is expected to be the dominant length scale in determining the upstream induced pressure field. Since the layer thickness is itself proportional to the plate length, it may not be possible to eliminate this effect.

This mechanism is analyzed for a two-dimensional, supersonic turbulent boundary layer on a finite length flat plate with injection rates approaching the constant pressure mixing layer entrainment rate (blow-off). The integral moment method of Lees and Reeves[5] (modified for turbulent flow) is employed to include the important interaction between the viscous and inviscid flows. The velocity integrals which appear in the equations are derived from data obtained in constant pressure flow experiments,[6] and form the equivalent of the Falkner-Skan profiles used by Lees and Reeves[5] to characterize their integrals.

As injection is increased, the velocity profiles become inflected and the sonic line moves away from the wall. Within the context of the integral theory, increasing injection results in a flow which goes "subcritical."[5] This behavior is the central concept of this analysis, because under this condition the effect of termination of injection can be felt upstream of the end of injection.

The saddle point which occurs at the end of injection is approximated by a "sink-type" singularity in the equations. The approximation, which is not central to the analysis, allows for rapid numerical solutions. By providing for this singularity, solutions can then be obtained which require no adjustable constants.

Section 2 presents a derivation of the governing equations, and the compressibility transformation employed. Section 3 outlines the analytical approach used to treat the flow in the vicinity of the end of injection. Finally, in Sec. 4, the results of the computations are compared with the experimental data and conclusions are drawn for higher injection rates.

2. Governing Equations

2.1 Derivation and Transformation of the Equations

The equations for the mean flow quantities are assumed to be the boundary-layer equations of a perfect gas (γ, C_p = const) with a constant total temperature

$$(\rho u)_x + (\rho v)_y = 0 \tag{1}$$

$$\rho u u_x + \rho v u_y = \tau_y - P_x \tag{2}$$

$$P_y = 0 \tag{3}$$

$$C_p T + u^2/2 = C_p T_e + U_e^2/2 = \text{const} \tag{4}$$

where the subscript e refers to quantities at the edge of the viscous layer. The assumption of constant total temperature is not a necessary one but is consistent with the data to be predicted.[6]

Equations (1) and (2) and the equation obtained by multiplying Eq. (2) by u are now integrated across the layer ($y = 0 - \delta$) to give (for isentropic external flow)

$$\tan\Theta \equiv v_e/u_e = d\delta^*/dx + [(\delta^* - \delta)/\rho_e u_e] \times (d/dx)\rho_e u_e + \lambda_e \tag{5}$$

$$(1/\rho_e u_e^2)(d/dx)(\rho_e u_e^2 \theta) + (\delta^*/u_e)(du_e/dx) = \lambda_e[1 + C_f/2\lambda_e] \tag{6}$$

$$\frac{1}{\rho_e u_e^3}\frac{d}{dx}(\rho_e u_e^3 \theta^{**}) + \frac{2}{u_e}\frac{du_e}{dx}\{\delta^* - \delta_u\} = \lambda_e\left[1 + \frac{2}{\lambda_e}\int_0^\delta \frac{\tau}{\rho_e u_e^2}\frac{\partial(u/u_e)}{\partial y}\,dy\right] \tag{7}$$

where subscripts e refer to quantities at the edge ($y = \delta$) and subscripts w refer to wall values. Here $\lambda_e = \rho_w v_w/\rho_e u_e$, $C_f/2 = \tau_w/\rho_e u_e^2$ and δ^*, θ and θ^{**} are defined by

$$\delta^* = \int^\delta \left(1 - \frac{\rho u}{\rho_e u_e}\right) dy, \qquad \theta = \int_0^\delta \frac{\rho u}{\rho_e u_e}\left(1 - \frac{u}{u_e}\right) dy$$

$$\theta^{**} = \int_0^\delta \frac{\rho u}{\rho_e u_e}\left[1 - \left(\frac{u}{u_e}\right)^2\right] dy \tag{8}$$

$$\delta_u = \int_0^\delta \left(1 - \frac{u}{u_e}\right) dy$$

At this point, in Eq. (6) it is assumed that in the blowing region $C_f/2\lambda_e \ll 1$ and this term is neglected. However, the last term in Eq. (7) which represents the turbulent dissipation is retained since mixing is assumed to be important in the layer, although wall shears are negligible.

Now Eqs. (5–7) are to be transformed into an equivalent low-speed form in order to remove the implicit Mach number dependence from the integral properties appearing in the equations. In order to do this, (following Stewartson[7]), define a variable $dY = (a_e\rho)/(a_2\rho_2)dy$, where the subscript 2 refers to some reference point in the flow (which will be taken to be the similar region upstream of the end of injection where $dP/dx = 0$).

Using this transformation and manipulating the equation, one obtains for constant total temperature

$$B\frac{d\delta_i^*}{dx} + \delta_i^*\frac{d\mathfrak{IC}}{dx} + f\frac{\delta_i^*}{M_e}\frac{dM_e}{dx} = \frac{a_e\rho_e}{a_2\rho_2}\left[\frac{\tan\Theta}{m_e} - \frac{\lambda_e}{m_e}\right] \tag{9}$$

$$\mathfrak{IC}\frac{d\delta_i^*}{dx} + \delta_i^*\frac{d\mathfrak{IC}}{dx} + (2\mathfrak{IC} + 1)\frac{\delta_i^*}{M_e}\frac{dM_e}{dx} = \lambda_e\left(\frac{\rho_e a_e}{\rho_2 a_2}\right) \tag{10}$$

$$J\frac{d\delta_i^*}{dx} + \delta_i^*\frac{dJ}{dx} + \frac{3J\delta_i^*}{M_e}\frac{dM_e}{dx} = \lambda_e[1 + R]\left(\frac{\rho_e a_e}{\rho_2 a_2}\right) \tag{11}$$

where

$$B = \mathfrak{IC} + (1 + m_e)/m_e \text{ and } m_e = [(\gamma - 1)/2]M_e^2$$

$$f = \left[2 + \frac{\gamma + 1}{\gamma - 1}\left(\frac{m_e}{1 + m_e}\right)\right]\mathfrak{IC} + \left[\frac{M_e^2}{m_e(1 + m_e)}\right]Z + \frac{3\gamma - 1}{\gamma - 2}$$

$$Z = \frac{1}{\delta_i^*}\int_0^{\delta_i}\frac{u}{u_e}\,dY; \quad J = \frac{1}{\delta_i^*}\int_0^{\delta_i}\frac{u}{u_e}\left[1 - \left(\frac{u}{u_e}\right)^2\right] dY \tag{12}$$

$$\delta_i^* = \int_0^{\delta_i}\left(1 - \frac{u}{u_e}\right) dY; \quad \theta_i = \int_0^{\delta_i}\frac{u}{u_e}\left(1 - \frac{u}{u_e}\right) dY$$

$$\mathfrak{IC} = \frac{\theta_i}{\delta_i^*}; \quad R = \frac{2}{\lambda_e}\int_0^{\delta_i}\frac{\tau}{\rho_e u_e^2}\frac{\partial(u/u_e)}{\partial Y}\,dY$$

Now it must be shown that the integral functions Z, J, and R which appear in Eqs. (9–11) are not implicitly dependent on Mach number.

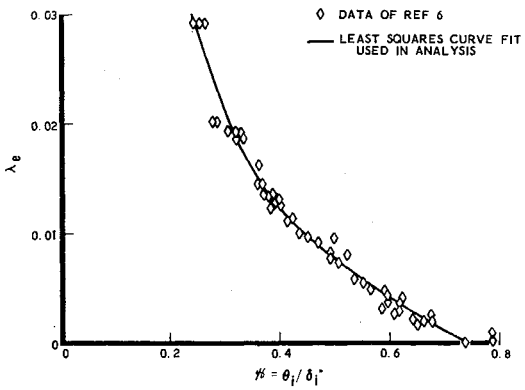

Fig. 1 Curve fit of data for $\mathcal{H}$ in similar region.

This can be done by recalling the transformation of Coles[8] for turbulent flow;

$$\bar{\psi} = \sigma(x)\psi \tag{13}$$

$$d\bar{x} = \xi(x)dx \tag{14}$$

$$\bar{\rho}\partial\bar{y} = \eta(x)\rho\partial y \tag{15}$$

where σ, ξ, η are three unknown scaling functions.§ An immediate consequence of Eqs. (13–15) has been shown by Coles[8] to be that at corresponding points in the flow for any $\eta(x)$, $u/u_e = \bar{u}/\bar{u}_e$. Since the quantities Z and J are formed by ratios of integrals over the transformed variable $\bar{Y}$ and the integrals involve only velocity ratios, $u/u_e = \bar{u}/\bar{u}_e$, these functions are already in a form independent of density effects and are independent of the choice of $\eta(x)$.

The argument for R is somewhat more complicated. In general, the quantity R which appears in Eq. (11) does not transform in a simple manner. However, if the effect of wall shear can be neglected, it can be shown (see Appendix A) that the quantity $(\tau/\rho_e u_e^2)/\lambda_e$ is an invariant under the transformation (13–15) at corresponding stations for constant pressure flows. Then, the integral R is indeed independent of density or of the choice of $\eta(x)$. Hence, the integrals R, J, and Z which appear in Eqs. (9–11) are density invariant at corresponding points in the two flows.

The problem now becomes one of determining what is meant by "corresponding points." That is, what is the relationship between λ_e and $\bar{\lambda}_e$, the injection rates in the compressible and incompressible flows?

This information is provided by the experimental data. As was shown in Ref. 6, the velocity profiles for both the incompressible and compressible flows (u/u_e vs $\bar{y}/\bar{\theta}$) can be shown to agree for large injection and constant pressure at $\lambda_e = \bar{\lambda}_e$, where λ_e, $\bar{\lambda}_e$ are the ratio of mass flow per unit area at the wall to that at the edge for the compressible and incompressible flows, respectively. Hence, $\lambda_e = \bar{\lambda}_e$ characterizes the corresponding points in the two flows for large injection with

$$C_f/\lambda_e \ll 1; \quad \bar{C}_f/\bar{\lambda}_e \ll 1$$

where C_f, $\bar{C}_f$ are the skin-friction coefficients in the two flows.

Now, it is assumed that this relationship holds ($\lambda_e = \bar{\lambda}_e$) even when the pressure is not constant, i.e., the compressibility transformation is not affected by the pressure gradient.

Furthermore, at this point it is assumed that the quantities Z, R, and J appearing in Eqs. (9–11) can be expressed as functions of one-parameter $\mathcal{H} = \theta_i/\delta_i^*$, and that the functional dependence can be obtained from the constant pressure similar flow solutions (experiments). A one-parameter representation is valid if in this region there is only one scale to the problem. However, the region downstream of injection, where wall viscosity effects again become important probably requires a two-parameter representation.

Finally, a relation between M_e and $\tan\Theta$ is needed to complete the set of equations. Following Lees and Reeves,[5] since this is expected to be an expansion starting from a uniform flow region, Prandtl-Meyer flow is assumed. Then, the relation between induced flow angle and Mach number is

$$\Theta(x) - \Theta(x_2) = \int_{M_e}^{M_2} \frac{(M^2-1)^{1/2}}{1 + [(\gamma-1)/2]M^2}\frac{dM}{M} \tag{16}$$

where $\Theta(x_2)$ is the induced inviscid flow angle in the similar region, which can be calculated as shown in Ref. 2.

Equations (9–11) together with the relation Eq. (16) and the definitions (12) form a set of three ordinary differential equations for the three unknowns M_e, δ_i^*, $\mathcal{H}$. Once these are obtained, the pressure and physical displacement thickness can be computed by standard methods.

It is important to note at this point that in the constant pressure region where $\mathcal{H}$, M_e are constant, $\mathcal{H}$ is directly determined as a function of λ_e. In the nonsimilar region near the end of injection, however, the profile will be "unhooked" from λ_e. That is, the dependence of J, $dJ/d\mathcal{H}$, Z, R, on $\mathcal{H}$ is maintained, but now $\mathcal{H}$ is obtained from a solution of the three Eqs. (9–11).

2.2 Evaluation of Integral Functions

In the similar flow regime, M_e, $\mathcal{H}$ = constant, Eqs. (9–11) reduce to

$$B(d\delta_i^*/dx) = (1/m_e)[\tan\Theta - (\rho_w v_w/\rho_2 u_2)] \tag{17}$$

$$\mathcal{H}(d\delta_i^*/dx) = \rho_w v_w/\rho_2 u_2 \tag{18}$$

$$J(d\delta_i^*/dx) = (\rho_w v_w/\rho_2 u_2)(1 + R) \tag{19}$$

$\mathcal{H}$, J, and Z are calculated from the measured velocity profiles[6] with minimum error. However, a direct calculation of R is difficult since it involves differentiating experimental data. Therefore R was evaluated by combining Eq. (18) and (19) to give

$$R = J/\mathcal{H} - 1 \tag{20}$$

so, for any $\mathcal{H}$ and J, R is determined.

Since there is some scatter in the experimental data for, say, J, and Z in the experiments,[6] the results obtained have been approximated with a least square fit. $dJ/d\mathcal{H}$ was ob-

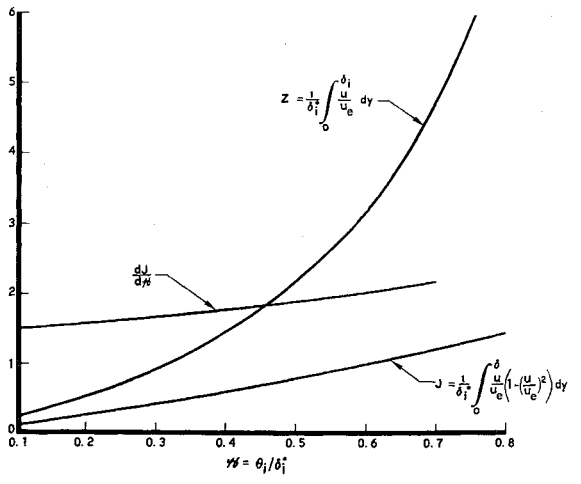

Fig. 2 Integral functions z, J, dJ/d H vs $\mathcal{H}$.

§ As pointed out by Coles,[8] these equations represent sufficient conditions and make no assumption as to the nature of the shear stress function, τ, or of the energy equation. Their restriction lies in the assumption of boundary-layer equations. In order to specify the functions and hence the transformation, more information about these quantities is necessary.

tained by spline fitting the curve of J vs $\mathfrak{IC}$ and then least square fitting the resulting derivatives. Figure 1 presents the curve for $\mathfrak{IC}$ obtained from the data of Ref. 6 as a function of λ_e, the injection parameter. Included in Fig. 1 is the data of Ref. 6 to give an indication of the experimental scatter previously mentioned. Figure 2 presents the quantities Z, J, and $dJ/d\mathfrak{IC}$ as a function of $\mathfrak{IC}$ obtained as indicated above. R is calculated from Eq. (20) and, using Fig. 2, can be expressed as a function of $\mathfrak{IC}$, only.

A point worth mentioning at this stage is that if the eddy viscosity model proposed by Lees and Chapkis[2] is assumed, and the reference density is taken to be equal to the edge value, the only term which changes in Eqs. (9–11) is R. For their formulation[2]

$$R = K_\theta \mathfrak{IC} R'/\lambda_e$$

where

$$R' = \delta_i^* \int_0^{\delta_i} G\left(\frac{Y}{\theta_i}\right)\left[\frac{\partial(u/u_e)}{\partial Y}\right]^2 dY$$

With an eddy viscosity formulation, R', J can be obtained as a function of $\mathfrak{IC}$ from the resulting similar equation regardless of the value of K_θ. Then, if one uses the experimental curve of $\mathfrak{IC}$ vs λ_e, K_θ can be obtained from

$$K_\theta(\lambda_e) = [\lambda_e/2\mathfrak{IC}(\lambda_e)R'(\mathfrak{IC})]\{[J(\mathfrak{IC})/\mathfrak{IC}(\lambda_e)] - 1\} \quad (21)$$

Figure 3 presents the resulting curve obtained using the experimentally determined curve of $\mathfrak{IC}$ as a function of λ_e and the integral functions J and R' obtained from the similar solutions of Lees and Chapkis.[2¶] It is interesting to note that K_θ thus obtained is a slight function of λ_e, and at high injection rates seems to be approaching the free shear layer value ($K_\theta \approx 0.045$). However, some caution is necessary at this point in interpreting this trend in K_θ, since a distribution function $G(Y/\theta_i)$ for the variation of the eddy viscosity across the layer was assumed, a priori, by Lees and Chapkis[2] in their formulation. The form chosen for this variation influences the value of K_θ obtained using Eq. (21). In fact, Fig. 4 shows the experimentally determined variation of normalized eddy viscosity as calculated from the experimental velocity profiles of Ref. 6. In obtaining the results shown in Fig. 4, a five-point smoothing was used. A quartic was least squares fitted to successive sets of points and the derivative was calculated for the central point in a set by differentiating the resulting polynomial. The shear stress was calculated by integrating the momentum equation using experimental velocity profiles, as shown in Ref. 6, and the

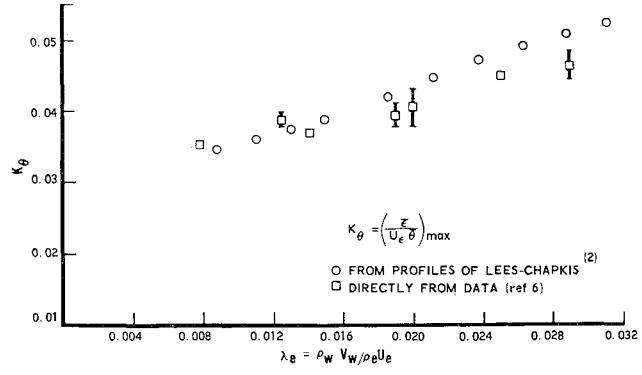

Fig. 3 Variation of K_θ with λ_e.

¶ Also included in Fig. 3 is the value of K_2 obtained by directly evaluating the eddy viscosity from the experimental data and taking K_2 to be the maximum value in the layer. In view of the errors involved in differentiating experimental data, the agreement can be considered quite good.

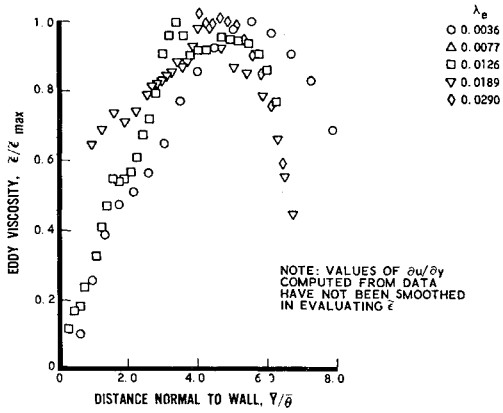

Fig. 4 Eddy viscosity variation through layer.

eddy viscosity was obtained from $\epsilon = (\tau/\rho)(\partial u/\partial y)$. Although there is considerable scatter, it appears as if $\tilde{\epsilon}/\tilde{\epsilon}_{max}$ certainly varies across the layer with a roughly parabolic shape. Hence, the approach taken from here on is to use the integral functions determined as shown previously without employing an eddy viscosity model. As a sidelight, however, the results presented in Figs. 1 and 3 can be combined as shown in Fig. 5, to present K_θ as a function of $\mathfrak{IC}$. In Figure 5 the data obtained by Bradshaw[12] for low-speed equilibrium flows with adverse pressure gradients and Liepmann and Laufer[13] for a mixing layer are also included. The coincidence of these results suggests the possibility of using the observed variation of K_θ with $\mathfrak{IC}$ for flows with combined pressure gradient and mass transfer.

3. Analytical Considerations

3.1 Subcritical-Supercritical Behavior of Equations

Under certain conditions the effect of a disturbance in a boundary layer can be felt upstream of the point of disturbance through the coupling of the inviscid pressure field and the viscous flow. Within the framework of the integral formulation, the flow can be divided into two regions, subcritical and supercritical. Subcritical flows exhibit an upstream sensitivity to disturbances while supercritical flows do not.

The boundary can be obtained by considering Eqs. (9–11) as a set of linear algebraic equations for the three derivatives (here, primes denote differentiation with respect to $\mathfrak{IC}$)

$$(\delta_i^*/M_e)dM_e/dx = N_1(M_e,\mathfrak{IC})/D(M_e,\mathfrak{IC}) \quad (22)$$

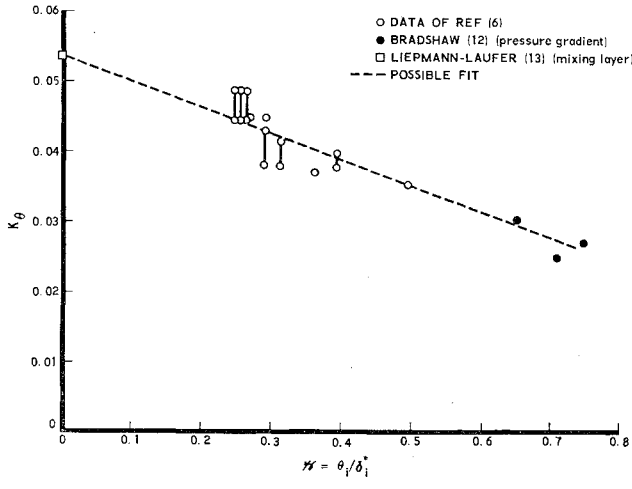

Fig. 5 Variation of K_θ with $\mathfrak{IC}$.

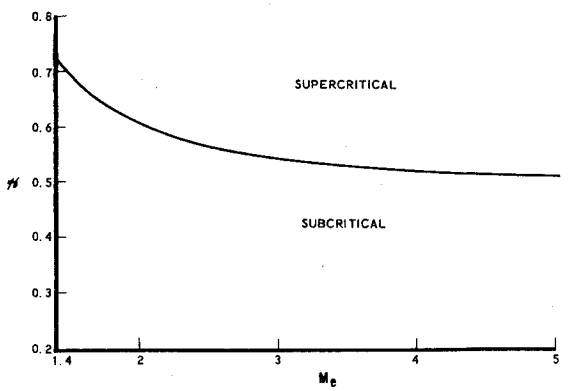

Fig. 6 Critical line, $D(M_e, \mathcal{H}) = 0$.

$$\delta_i^* d\mathcal{H}/dx = N_2(M_e,\mathcal{H})/D(M_e,\mathcal{H}) \quad (23)$$

$$d\delta_i^*/dx = N_3(M_e,\mathcal{H})/D(M_e,\mathcal{H}) \quad (24)$$

where, in this case

$$N_1 = \frac{a_e\rho_e}{a_2\rho_2}\frac{\tan\Theta}{m_e}(\mathcal{H}J' - J) + \lambda_{e_2}\frac{M_2}{M_e}\left\{\frac{1+m_e}{m_e} - \frac{(\mathcal{H}J' - J)}{m_e} - (BJ' - J)\right\} + R\lambda_{e_2}\frac{M_2}{M_e}\left(\frac{1+m_e}{m_e}\right) \quad (25)$$

$$N_2 = \frac{\tan\Theta}{m_e}\frac{a_e\rho_e}{a_2\rho_2}J(1-\mathcal{H}) + \lambda_{e_2}\frac{M_2}{M_e}\times \left\{3JB - (2\mathcal{H}+1)B + \frac{3\mathcal{H}J}{m_e} + f\mathcal{H} - \frac{(2\mathcal{H}+1)J}{m_e} - fJ\right\} + R\lambda_{e_2}\frac{M_2}{M_e}\{f\mathcal{H} - B(2\mathcal{H}+1)\} \quad (26)$$

$$N_3 = \frac{\tan\Theta}{m_e}\frac{a_e\rho_e}{a_2\rho_2}\{3J - J'(2\mathcal{H}+1)\} + \lambda_{e_2}\frac{M_2}{M_e}\times \left\{(2\mathcal{H}+1) - f(1-J') - 3J - \frac{3J - (2\mathcal{H}+1)J'}{m_e}\right\} + R\lambda_{e_2}\frac{M_2}{M_e}\{2\mathcal{H}+1-f\} \quad (27)$$

$$D = f\{\mathcal{H}J' - J\} - J(\mathcal{H}-1) + B\{3J - (2\mathcal{H}+1)J'\}; \quad \lambda_{e_2} = \rho_w v_w/\rho_2 u_2 \quad (28)$$

As shown by Lees and Reeves[5] and Klineberg,[9] the curve $D(M_e,\mathcal{H}) = 0$ is the dividing line between super- and subcritical flows. For values of M_e, $\mathcal{H}$ on one side of this line the end of injection will have no calculable effect on the flow upstream of the termination and for values on the other side an effect will be observed. If the integral quantities are known as a function of $\mathcal{H}$ in Eq. (28), then this dividing line can be obtained by iteration. Figure 6 is a plot of the critical line for this flow. Note that the results shown in Fig. 6 do not depend on λ_e and, hence, do not depend on the compressibility transformation employed. Since the problem under consideration starts with a similar flow (N_1,N_2 = 0), then initially, $\mathcal{H}$ is known as a function of λ_e and Fig. 7 shows the critical line in this manner. Finally, since the similar region is characterized by a straight shock (linear growth), then Eqs. (17) and (18) can be combined to give the critical line in terms of freestream values, $\lambda_\infty = \rho_w v_w/\rho_\infty u_\infty$ and M_∞, by using the shock relations to obtain $\Theta(x_2)$ and solving these equations by an iteration process (Fig. 8). Note that in performing these calculations (Figs. 7 and 8) the crucial step is to establish a relationship between $\mathcal{H}$ and λ_e. Hence, as is seen from Fig. 8 at $M_\infty = 2.6$, any $\lambda_\infty \gtrsim 0.007$ will result in a flow which has a finite region near the end of the porous plate that is influenced by termination of injection.

With the subcritical nature of the flow established for a given freestream Mach number, the next question is how to obtain a solution to Eqs. (22–24).

3.2 Analogy with Flow around a Corner

One expects the effect of the end of injection to be similar to that for a flow effectively approaching a sharp expansion corner. That is, for an initially subcritical flow on the porous plate, the end of injection should cause a rapid expansion of the flow [an effective "corner"—as shown by Eq. (9)]. However, as shown by Victoria,[11] the viscous-inviscid interaction smooths out a "sharp" corner, and the transition from subcritical to supercritical flow (saddle-point singularity) occurs there. In Eqs. (22–27), both D and $N_i \to 0$ as the "corner" is approached, but $N_i/D \gg 1$ on the upstream side until one is very close to the corner. This observation provides a justification of the approximate method utilized by Ko and Kubota[10] for a sharp corner. In their method, $D \to 0$ while N_i remains finite, and they seek a solution of the moment equations with an integrable singularity (branch point) at the corner. Victoria's comparison of the branch-point and saddle-point solutions shows good agreement between these two solutions. In view of the complications involved in seeking the saddle point near the end of injection, the simpler approach of Ko and Kubota is used in the present analysis. Hence, consider solutions to Eqs. (22-24) which possess integrable, sink-type singularities in the gradients of M_e, $\mathcal{H}$, δ_i.** This should be a valid

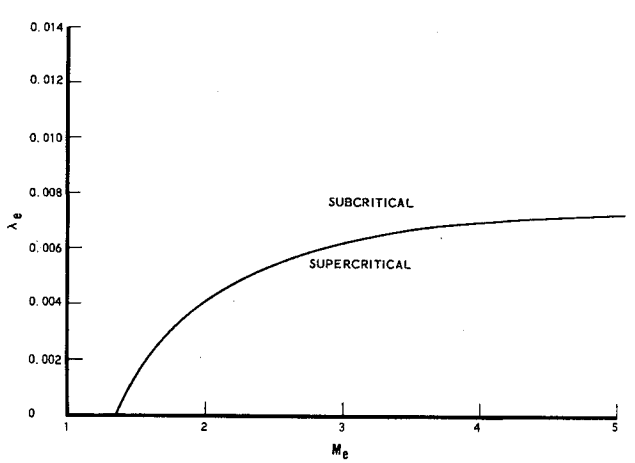

Fig. 7 Critical line, $D(M_e, \mathcal{H}) = 0$.

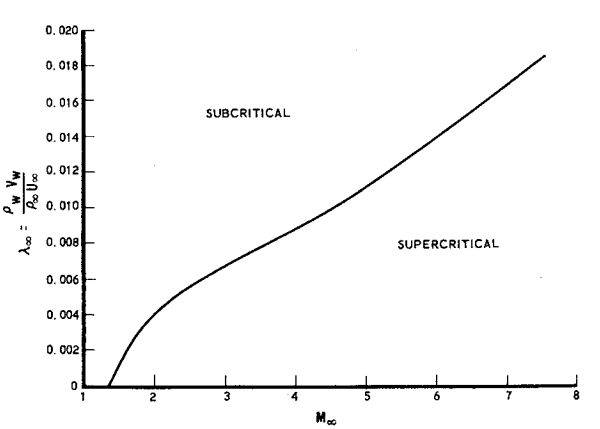

Fig. 8 Critical line, $D(M_e, \mathcal{H}) = 0$.

** Note that this is only an approximation. There is an essential difference between the singular points of these equations (where derivatives are finite) and a solution with a singularity at a point.

approximation if the flow becomes supercritical very near the end of injection.

3.3 Existence of a Singular Solution

Two questions have yet to be answered for the Eqs. (22–24) before the solutions can be obtained in a logical fashion. The first is whether solutions of the type required exist for these equations and the second is to establish a consistent method of obtaining these solutions numerically. Fortunately, the similarity between these equations and those treated by Ko and Kubota[10] make the answer to the first question quite straightforward to obtain. If one looks for solutions where

$$dM_e/dx \sim (L - x)^{-\alpha},\ d\delta_i^*/dx \sim (L - x)^{-\beta}$$
$$d\mathcal{H}/dx \sim (L - x)^{-\gamma} \tag{29}$$

near $x = L$, then requiring finite $\mathcal{H}_L$, M_{eL}, δ_{iL}^* at $x = L$ means that $0 < \alpha, \beta, \gamma < 1$ is necessary. By linearizing the equations about $\mathcal{H}_L$, M_{eL}, δ_{iL}^* it can be shown that to lowest order $\alpha = \beta = \gamma = \frac{1}{2}$. Then

$$M_e = M_{eL} - k_1(L - x)^{1/2},\ \mathcal{H} = \mathcal{H}_L - k_2(L - x)^{1/2}$$
$$\delta_i^* = \delta_{iL}^* + k_3(L - x)^{1/2} \qquad x \leq L \tag{30}$$

near $x = L$, where k_1, k_2, and k_3 are positive constants which can be obtained in terms of conditions at $x = L$. Hence, solutions with a sink-type behavior exist for Eqs. (22–24).

The second question involves the determination of a consistent perturbation procedure for obtaining these solutions starting with a similar flow (M_e, $\mathcal{H}$ = constant). In the vicinity of the end of injection, a small but relatively rapid change occurs in the boundary layer and the perturbation in the external flow must be considered simultaneously with that in the boundary layer. Assuming $\epsilon = [(\gamma - 1)/2]^2 M_2^3 \lambda_{e_2} \ll 1$,†† then the analysis of Ko and Kubota[10] for laminar flow can be directly applied to this problem. Assuming the change takes place over a small scale, let $\hat{x} = (x - x_2)/\epsilon$ where $\hat{x}$ is assumed order 1; $x - x_2 \ll 1$. That is, assume the change takes place over a distance of order $M_2^3\ \lambda_{e2}$ which, for hypersonic flow with large injection, is of order (Mach number) $\times$ (boundary-layer thickness), so boundary-layer equations are still applicable. For supersonic flow, the dependence of boundary-layer thickness on Mach number is more complicated but is less than M_2^2. In this case, the validity of the boundary-layer equations may be questionable.

Near the similar flow region (subscripts 2), let

$$\delta_i^* = \delta_{i_2}^* + \sigma\hat{\delta},\ \mathcal{H} = \mathcal{H}_2 + \sigma\hat{\mathcal{H}},\ M_e = M_2 + \sigma\hat{M} \tag{31}$$

where $\sigma \ll 1$ and $\hat{}$ quantities are assumed of O(1). Then a substitution of Eq. (31) into the Eqs. (22–24) yields directly, to lowest order

$$\hat{\delta}/\delta_{i_2}^* = -K[(1 + 2\mathcal{H}_2)J_2' - 3J_2],\quad \hat{\mathcal{H}} = K[(1 - 2)J_2]$$
$$M/M_2 = K[\hat{\mathcal{H}}_2 J_2' - J_2] \tag{32}$$

where K represents an arbitrary, but small, perturbation of the similar flow variables, $\mathcal{H}_2$, M_{e_2}, $\delta_{i_2}^*$, i.e., Eq. (32) relates the change in any two variables if one is given small change. This result is the same as that obtained by Ko and Kubota[10] and Victoria[11] for laminar flow for weak interaction where $(\gamma - 1/2)^2 M_\infty^3/(Re_x)^{1/2} = (\gamma - 1/2)^2\chi \ll 1$ is assumed. The analogy to the corner solution of Eqs. (10) and (11) requires that in our case $(\gamma - 1/2)^2 M_2^3 \lambda_e \ll 1$. So, in flows with large injection, the analogue of χ is $M_e^3\lambda_e$.

4. Results

4.1 Numerical Solution and Comparison with Experiment

With the background presented, the Eqs. (22–24) can now be integrated in a systematic way to the end of the porous plate. An important point to note in this problem is that, unlike the laminar flow case, in Eqs. (22–24), N_1, N_2, and N_3 are only functions of M_e and $\mathcal{H}$. Hence, the equations are invariant to an affine transformation $\tilde{x} = x/x_2$, $\tilde{\delta} = \delta_i^*/x_2$. This means that at the beginning of the integration x_2 can be chosen arbitrarily. Then, using the perturbations on δ_i^*, $\mathcal{H}$, M_e from the similar solution, a solution is generated which has a proper behavior. Numerically this is accomplished by picking a positive value of K so that the solution obtained corresponds to an expansion (M_e, $\mathcal{H}$ increasing, δ_i^* decreasing).‡‡ At the point where, say $d\mathcal{H}/dx$ gets larger than a predetermined number, the solution is continued by simply considering x as a function of $\mathcal{H}$ and inverting the integration procedure. Since neither N_1, N_2, or $N_3 \to 0$, the solution then proceeds smoothly. The singular point can then be rightly called the plate length, L. Computed pressure variations obtained in this way can be plotted solely as a function of x/L for any set of freestream Mach number and injection rate.

Solutions were obtained for three of the higher injection rates used in the experiments using a 7094 computer and standard integration routines. The results are shown in Fig. 9 and compared with the experimentally observed pressure distribution. The agreement is fairly good although significant values of dP/dy are observed close to the corner in the experiments and the equations do not provide for dP/dy. At the highest injection rate the theory seems to somewhat overpredict the observed pressure gradient. More importantly, the simple one-parameter representation seems to predict accurately the scale of upstream influence in pressure produced by termination of injection. In fact, for the highest injection rate, a good portion of the plate is strongly influenced by the finite length effect. Fig. 10 presents a comparison between the observed and predicted variation of the form parameter, $\mathcal{H}$, for an intermediate injection rate.§§ The disagreement in the region near the beginning of the porous plate is caused by the fact that in the experiment a finite thickness boundary layer is present at the start of injection, while the theory assumes zero initial boundary-layer thickness. The observed initial variation in is, then, the adjustment of the initial boundary layer to the injection. Conceivably, this effect might be amenable to analysis using ideas similar to those employed herein.

4.2 Implication of the Analytical Results

The analysis presented herein indicates some rather startling conclusions. First, as indicated by the equations, for large injection where $C_f/\lambda_e \ll 1$, the solutions are functions only of x/L. This means that experimentally, a doubling of porous plate length will not decrease the fraction of

†† The assumption $[(\gamma - 1)/2]^2 M_2^3 \lambda_{e_2} \ll 1$ is not as restrictive as it may first appear to be. For hypersonic flow, Lees[2] has shown that even for $M_\infty^2\lambda_\infty \gg 1$ the induced flow angle in the similar region, Θ, approaches a limiting value where $\Theta \sim \lambda_e^{1/3}$. Since in this case $M_2 \sim 1/\theta$, the quantity $[(\gamma - 1)/2]^2 M_2^3\lambda_{e_2}$ approaches a constant given by $\epsilon_{\max} \to [\gamma(\gamma - 1)/2]^{1/2}$. For $\gamma = 1.4$, $\epsilon_{\max} \approx 0.53$, and $\epsilon_{\max}^2$ is small compared to unity. Hence, this perturbation scheme can be expected to work for most of the Mach numbers and injection rates of interest.

‡‡ Note, also, that since N_1, N_2, N_3 do not depend on δ_i^*, the equations can be solved without reference to the particular value of K chosen. That is, the effect of varying K can be scaled out of the solution as long as K is small so that the relations [Eq. (32)] are valid.

§§ Similar results for $\lambda_\infty = 0.026$ and 0.043 were not obtained during the experiments of Ref. 6 due to the errors involved in reducing Pitot data. In the region where $\partial P/\partial x$ was observed, enough $\partial P/\partial y$ was noticeable to render accurate reduction of the data impossible.

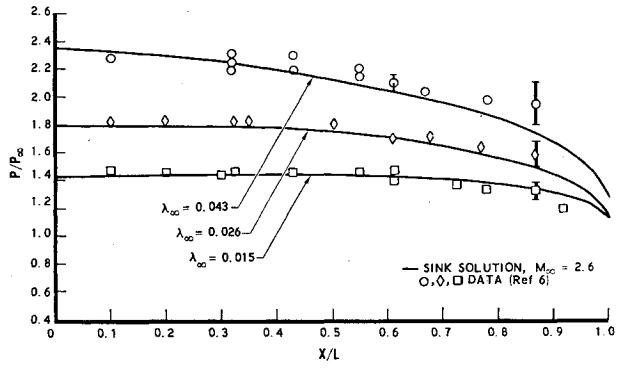

Fig. 9 Comparison of "sink solution with data."

plate influenced by this downstream effect. That is, since the similar layer grows linearly and since the only scale height in the equations is δ^*, the effect will scale with this height and thus always cover the same percentage of plate. Of course, the absolute length of similar region is increased but only in proportion to the length of plate. The second effect is shown more clearly in Fig. 11, where a parametric study has been performed for various injection rates. Here it becomes clear that, at least at $M_\infty = 2.6$, when $\lambda_\infty \approx 0.050$ which corresponds to $\lambda_e \approx 0.033$, virtually the entire plate is influenced by the pressure gradient produced by the termination of injection. This value of injection parameter approaches the entrainment rate of the incompressible constant pressure free shear layer (expected to be the "blow-off" value for the turbulent boundary layer). It is not expected that solutions would exist for constant pressure beyond this value. However, if the turbulent flow solutions behave like the laminar ones, then the analysis presented in Ref. 4 would indicate that no singularity will be observed for any small negative pressure gradient and such a pressure gradient has been provided by the effect of termination of injection.

Moreover, the laminar solutions of Ref. 4 indicated that, for adiabatic flow at values of injection parameter about twice the value which would normally "blow off" the zero pressure gradient boundary layer, the lowest-order asymptotic solutions (which are essentially an inviscid flow approximation) give a valid representation of the flow.¶¶ For the turbulent case, one would expect that at $M_\infty \approx 2.6$ for adiabatic flow, an inviscid flow model will adequately characterize most of the flow for $\lambda_\infty \gtrsim 0.1$ ($\lambda_e \gtrsim 0.06$). If the effect of compressibility observed on $M_\infty = 2.6$ can

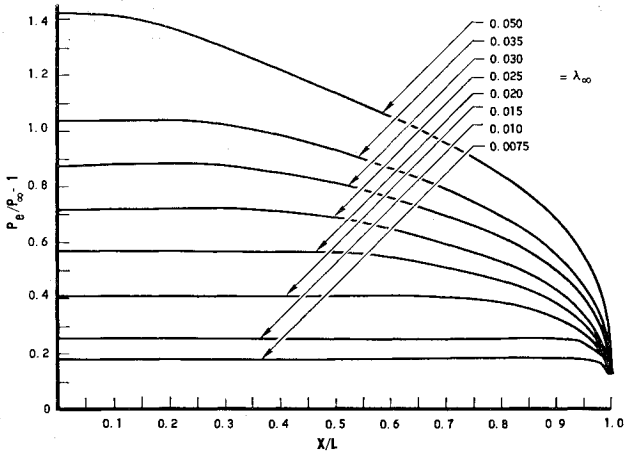

Fig. 10 Effect of termination of injection $M_\infty = 2.6$.

¶¶ For a cold wall, however, the effects of mixing will influence the flow to higher injection rates.

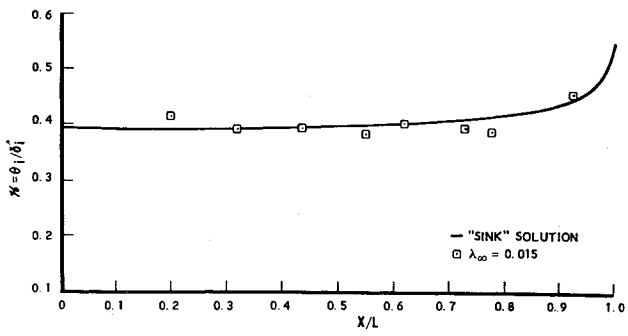

Fig. 11 Comparison of form parameter $M_\infty = 2.6$.

be used at very high Mach numbers, then at $M_\infty \gg 1$ for $\lambda_\infty \gtrsim 0.4$ ($\lambda_e \gtrsim 0.06$), the same should be true.* However, for injection rates this high at Mach numbers greater than 7 or 8, for adiabatic flow, the effect of the momentum of the injected gas will become important and may invalidate the neglect of $\partial P/Py$ in the analysis.

Hence, the analysis has provided the step which gives a quantitative estimate for the range of injection in turbulent flow where the effect of induced pressure gradient cannot be neglected. It also indicates that inviscid solutions for a semi-infinite plate with constant injection may not comprise a rational approximation to the physical flow. For constant injection, the proper two-dimensional limiting inviscid models would seem to be those which properly account for the discontinuity in boundary conditions which exists at the end of injection for any finite plate length.[3]

Appendix A: Transformation of Dissipation Integral R

For zero pressure gradient, Eqs. (A1) and (A2) become

$$(\rho u)_x + (\rho v)_y = 0 \tag{A1}$$

$$\rho u\, u_x + \rho v\, u_y = \tau_y \tag{A2}$$

Integrating (A1) from $y = 0$ to $y = \tilde{y}$

$$\frac{v}{u}(\tilde{y}) = \lambda_e\left(\frac{\rho_e u_e}{\rho u}\right) - \frac{\rho_e u_e}{\rho u}\frac{d}{dx}\left\{\int_0^{\tilde{y}} \frac{\rho u}{\rho_e u_e}\, dy\right\} + \frac{d\tilde{y}}{dx} \tag{A3}$$

For similar constant total temperature flow, $\rho u/\rho_e u_e = f(y/\theta)$ and $d\theta/dx \cong \lambda_e = \text{const}$, so Eq. (A3) gives

$$\frac{v}{u} = \lambda_e\left[\frac{\rho_e u_e}{\rho u} - \frac{\rho_e u_e}{\rho u}\int_0^{\tilde{y}/\theta} \frac{\rho u}{\rho_e u_e}\, d\left(\frac{y}{\theta}\right) + \frac{\tilde{y}}{\theta}\right] \tag{A4}$$

Similarly, integrating Eq. (A2) and using Eq. (A4), one gets

$$\frac{\tau - \tau_w}{\rho_e u_e^2} = \lambda_e\left\{\frac{u}{u_e} - \frac{u}{u_e}\int_0^{\tilde{y}/\theta} \frac{\rho u}{\rho_e u_e}\, d\left(\frac{y}{\theta}\right) + \int_0^{\tilde{y}/\theta} \frac{\rho u^2}{\rho_e u_e^2}\, d\left(\frac{y}{\theta}\right)\right\} \tag{A5}$$

where τ_w is the wall shear stress. Using Coles'[8] transformation functions, it follows that $d(\tilde{y}/\theta) = \rho/\rho_e d(y/\theta)$, $u/u_e = \bar{u}/\bar{u}_e$, hence, (A5) gives

$$(\tau - \tau_w)/\lambda_e \rho_e u_e^2 = (\tilde{\tau} - \tilde{\tau}_w)/\bar{\lambda}_e \bar{\rho}_e \bar{u}_e^2 \tag{A6}$$

at corresponding stations in the flows. Hence, if $C_f/2\lambda_e = C_f/2\lambda_e \ll 1$, the dissipation integral R is density invariant.

* It might be mentioned here that the above analysis is also applicable to laminar flow. In this case, one expects that the termination of injection will influence the flow for much smaller injection rates than ment oned herein, since the limiting value of entrainment for a laminar mixing layer is $O[1/(Re)^{1/2}]$.

References

[1] Catherall, D., Stewartson, K., and Williams, P. G., "Viscous Flow Past a Flat Plate with Uniform Injection," *Proceedings of the Royal Society of London, Ser. A*, Vol. 284, March 1965, pp. 370–396.

[2] Lees, L. and Chapkis, R., "Surface Mass Injection at Supersonic and Hypersonic Speeds as a Problem in Turbulent Mixing," *AIAA Journal*, Vol. 7, No. 4, April 1969, pp. 671–680; also AIAA Paper 68-130, New York, Jan. 1968.

[3] Thomas, P. E., "Compressible Flow Over a Finite Flat Plate with Massive Blowing," Rept. 61-78-68-8, March 1968, Lockheed Research Lab., Palo Alto, Calif.

[4] Kubota, T. and Fernandez, F. L., "Boundary-Layer Flows with Large Injection and Heat Transfer," *AIAA Journal*, Vol. 6, No. 1, Jan. 1968, pp. 22–58.

[5] Reeves, B. L. and Lees, L., "Supersonic Separated and Reattaching Flows: I. General Theory and Application to Adiabatic Boundary-Layer/Shock-Wave Interactions" *AIAA Journal*, Vol. 2, No. 11, Nov. 1964, pp. 1907–1920.

[6] Fernandez, F. L. and Zukoski, E., "Experiments in Supersonic Turbulent Flow with Large Distributed Surface Injection," *AIAA Journal*, Vol. 7, No. 9, Sept. 1969, pp. 1759–1767; also AIAA Paper 68-129, New York, Jan. 1968.

[7] Stewartson, K., "Correlated Incompressible and Compressible Boundary Layers," *Proceedings of the Royal Society*, A200, Dec. 22, 1949, London, pp. 84–100.

[8] Coles, D. F., "The Turbulent Boundary Layer in a Compressible Fluid," *The Physics of Fluids*, Vol. 9, 1964, p. 1403.

[9] Klineberg, J. M., "Theory of Laminar Viscous-Inviscid Interaction in Supersonic Flow," Ph.D. thesis, June 1968, California Institute of Technology, Pasadena, Calif.

[10] Ko, D. R. S. and Kubota, T., "Supersonic Laminar Boundary Layer along a Two-Dimensional Adiabatic Curved Ramp," *AIAA Journal*, Vol. 7, No. 2, Feb. 1969, pp. 278–304; also AIAA Paper 68-109, New York, Jan. 1968.

[11] Victoria, K. J., "Hypersonic Laminar Boundary Layer Near a Sharp Expansion Corner," Ph.D. thesis, 1969, California Institute of Technology, Pasadena, Calif.

[12] Bradshaw, P., "The Turbulence Structure of Equilibrium Boundary Layers," *Journal of Fluid Mechanics*, Vol. 29, 1967, Pt. A, pp. 625–645.

[13] Liepmann, H. W. and Laufer, J., "Investigation of Free Turbulent Mixing," TN 1257, Aug. 1947, NACA.

JULY 1970 AIAA JOURNAL VOL. 8, NO. 7

Nonequilibrium, Ionized, Hypersonic Flow over a Blunt Body at Low Reynolds Number

SANG-WOOK KANG*
Cornell Aeronautical Laboratory, Inc., Buffalo, N. Y.

Ionized nonequilibrium flow in the forebody region (downstream as well as the stagnation) of a catalytic blunt body is theoretically analyzed in the incipient merged-layer regime using the thin shock-layer assumption. The species conservation equations for seven species and six chemical reactions are considered; they are decoupled from the momentum and the energy equations. Nonsimilar solutions are obtained by application of an integral method approach for various degrees of rarefaction. The results show sizable effects of wall cooling and species diffusion on the dissociation and the ionization levels, demonstrating in the process that the inviscid flow analysis overpredicts the electron-density level by as much as two orders of magnitude in the stagnation region and by three orders of magnitude in the downstream region of a catalytic blunt body. In addition, the results suggest that the binary scaling principle may be applied to the case of an ionized merged-layer flow over a blunt body at high altitudes.

Nomenclature

a = body nose radius, cm
C_i = mass fraction of ith species, gm_i/gm of mixture
C_{pi} = specific heat at constant pressure of ith species, $cal/g_i - °K$
D_i = binary diffusion coefficient of ith species, cm^2/sec
E_i = surface-concentration gradient parameter of ith species, $\equiv (\partial C_i/\partial F)_b$
F = transformed normal coordinate, Eq. (12)
f = dimensionless stream function
G = parameter for shock standoff distance, Eq. (12)
H = total enthalpy, $h + (u^2 + v^2)/2$, cal/gm or atm-cm^3/g
h_i = static enthalpy of ith species, $h_i^0 + \int_0^T C_{pi}dT$, cal/g_i
h_i^0 = heat of formation of ith species, cal/g_i
h = static enthalpy, $\Sigma_i C_i h_i$, cal/g of mixture
j = unity for axisymmetric flow and zero for planar flow
k_{fj} = forward reaction rate for the jth reaction, $cm^3/mole_i$-sec
k_{bj} = backward reaction rate for the jth reaction, $cm^3/mole_i$-sec, or $cm^6/mole_i^2$-sec
K^2 = rarefaction parameter, $\epsilon(\rho_\infty U_\infty a/\mu)$
Le_i = Lewis number of ith species, Pr/Sc_i
m_i = molecular weight of ith species, g_i/g $mole_i$
n_i = mole fraction of ith species, C_i/m_i, $mole_i/g$ of mixture
N_0 = Avogadro's number, 6.025×10^{23} particles/mole
p = pressure, atm
Pr = Prandtl number
$\mathfrak{R}$ = universal gas constant, 82.06 atm-cm^3/gm mole − °K
r = distance from the axis to the body surface, cm
Sc_i = Schmidt number of ith species
T = temperature, °K
U = dimensionless streamwise velocity, $u/(U_\infty z)$
U_∞ = freestream velocity, cm/sec
u,v = velocities in physical coordinates (Fig. 1)
x,y = physical coordinates (Fig. 1)
z = r/a
β = shock angle
γ = specific heat ratio
Δ = shock standoff distance, cm
ϵ = $(\gamma - 1)/(2\gamma)$
Θ = total-enthalpy ratio, $(H - H_b)/(H_\infty - H_b)$

Received June 2, 1969; revision received December 11, 1969. This work was supported by NASA Goddard Space Flight Center, under Contract NAS 5-9978. The author wishes to acknowledge the useful discussions with M. G. Dunn and J. A. Lordi, and the assistance of J. R. Moselle in obtaining numerical solutions.

* Principal Engineer, Aerodynamic Research Department. Member AIAA.